Improving Small Molecule Generation using Mutual Information Machine

Danny Reidenbach[12*], **Micha Livne**[1*], **Rajesh K. Ilango**[1], **Michelle Gill**[1], **Johnny Israeli**[1]

[*] equal contributions, [1] NVIDIA, [2] UC Berkeley
dreidenbach@berkeley.edu, mlivne@nvidia.com, rilango@nvidia.com, mgill@nvidia.com, jisraeli@nvidia.com

Abstract

We address the task of controlled generation of small molecules, which entails finding novel molecules with desired properties under certain constraints (*e.g.*, similarity to a reference molecule). Here we introduce MolMIM, a probabilistic auto-encoder for small molecule drug discovery that learns an informative and clustered latent space. MolMIM is trained with Mutual Information Machine (MIM) learning, and provides a fixed length representation of variable length SMILES strings. Since encoder-decoder models can learn representations with "holes" of invalid samples, here we propose a novel extension to the training procedure which promotes a dense latent space, and allows the model to sample valid molecules from random perturbations of latent codes. We provide a thorough comparison of MolMIM to several variable-size and fixed-size encoder-decoder models, demonstrating MolMIM's superior generation as measured in terms of validity, uniqueness, and novelty. We then utilize CMA-ES, a naive black-box and gradient free search algorithm, over MolMIM's latent space for the task of property guided molecule optimization. We achieve state-of-the-art results in several constrained single property optimization tasks as well as in the challenging task of multi-objective optimization, improving over previous success rate SOTA by more than 5% . We attribute the strong results to MolMIM's latent representation which clusters similar molecules in the latent space, whereas CMA-ES is often used as a baseline optimization method. We also demonstrate MolMIM to be favourable in a compute limited regime, making it an attractive model for such cases.

1 Introduction

The lead optimization stage of the drug discovery process is time consuming, labor intensive, and has a high rate of failure, requiring as much as three years and hundreds of millions of dollars for a single drug. This stage is focused on optimizing candidate molecules using the design-make-test cycle, in which scientists design new molecules based on available assay information, synthesize these molecules, and then test them in new assays.

The risk and associated cost of this process makes it a high value automation task in the drug discovery pipeline (Kim et al. 2020; Engkvist et al. 2021). Successful solutions to the automated design of small molecules can be directly applied to related challenges associated with other biological modalities, such as protein design (Berenberg et al. 2022) and optimization of guide RNA sequence for CRISPR systems (Chuai et al. 2018).

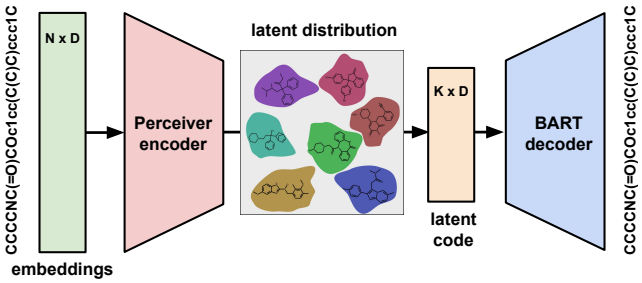

Figure 1: MolMIM is a probabilistic encoder-decoder model with a fixed-size representation that learns a latent distribution clustered around similar molecules. N is the token number, D is the embeddings dimension, K is the hidden length. Tokens are mapped to learnable embeddings.

Controlled generation of small molecules entails finding a new molecule with certain properties and under some constraints (e.g., similarity to a reference molecule, Vamathevan et al. (2019)). Often these molecules are represented in a text-based encoding format called SMILES (Weininger 1988). Efficient search of the space of molecules is a challenging problem due to the high dimensional and sparse nature of samples, where valid molecules are sparse given all possible combinations of legal characters in SMILES.

A common search method relies on genetic algorithms to modify a molecule's SMILES representation using heuristics. Examples would be random mutations and hand-crafted rules (Sliwoski et al. 2014; Mahmood et al. 2021). The complex and high dimensional search space often leads to low sampling efficiency of such methods. In addition, the search is often based on *ad hoc* rules which requires input from experts.

An alternative approach to automate this process with deep learning is to project the discrete molecules into a continuous space, wherein generation becomes sampling from a continuous space, and exploration becomes a manipulation of continuous vectors (Gómez-Bombarelli et al. 2018; Hoffman et al. 2022; Winter et al. 2019). Here, we follow that approach, focusing on learning a dense representation space that allows efficient sampling and exploration (Fig. 1).

In this paper we explore the effect of a bottleneck architecture and latent regularization methods on the ability to sample novel molecules, and on the performance of constrained optimization in the latent space. In more details, we explore the use of auto-encoder (AE, Goodfellow, Bengio, and Courville (2016)) with bottleneck, and two latent variable models, Variational auto-encoder (VAE, Kingma and Welling (2014)) and Mutual Information Machine (MIM, Livne, Swersky, and Fleet (2019)) which regularize the latent space. We show that all bottleneck models can offer superior sampling, as measured by validity, uniqueness, and novelty when compared to BART, which lacks a fixed-size representation. We also show how MIM learns a latent space which is particularly useful for finding novel molecules with target properties, especially under a limited compute regime.

Main contributions: We propose MolMIM, a novel probabilistic encoder-decoder model for SMILES data. The model is trained in an unsupervised manner without the need for denoising as part of the learning, reducing the number of training hyper-parameters. We demonstrate that MolMIM offers superior sampling capabilities when compared to BART, AE, and VAE. MolMIM learns an informative and clustered continuous representation of molecules which is particularly suitable for molecular property optimizations using a naive sampling-based CMA-ES algorithm (Hansen 2006). We emphasize that this level of molecule organization occurs without the use of molecular properties. We set multiple state-of-the-art results, demonstrating the effectiveness of the model in single and multi-property optimization.

2 Formulation

We focus here on denoising auto-encoders (Goodfellow, Bengio, and Courville 2016) where a corrupted input is encoded by an encoder into a latent code. The latent code is then used to reconstruct the original input by the decoder. More formally, we can describe auto-encoders (AE) in terms of encoding distribution $q_{\boldsymbol{\theta}}(\boldsymbol{z}|\boldsymbol{x})$ and decoding distribution $p_{\boldsymbol{\theta}}(\boldsymbol{x}|\boldsymbol{z})$, where we opt here for a probabilistic view. A deterministic encoder can be viewed as a Dirac delta function around the predicted mean. Given the encoder and decoder, the denoising AE (DAE) loss, per observation $\boldsymbol{x}$ can be expressed as,

$$\mathcal{L}_{\text{AE}}(\boldsymbol{\theta}) = \mathbb{E}_{\boldsymbol{z}\sim q_{\boldsymbol{\theta}}(\boldsymbol{z}|\tilde{\boldsymbol{x}})}\left[\log p_{\boldsymbol{\theta}}(\boldsymbol{x}|\boldsymbol{z})\right] \tag{1}$$

where $\boldsymbol{x} \in \mathcal{V}^N$ for vocabulary $\mathcal{V}$, $\tilde{\boldsymbol{x}}$ is some kind of corruption or augmentation of $\boldsymbol{x}$, $\boldsymbol{z} \in \mathbb{R}^H$, H is the hidden dimensions, and $\boldsymbol{\theta}$ is the union of all learnable parameters. Here we include the identity function in the set of augmentations, where $\tilde{\boldsymbol{x}} \equiv \boldsymbol{x}$.

Bottleneck BART Our baseline model is BART (Lewis et al. 2020), with data augmentation identical to Chemformer (Irwin et al. 2022). BART is a transformer-based seq2seq model that learns a variable-size hidden representation $H = |\tilde{\boldsymbol{x}}| \times D$. That is, the dimension of the hidden representation is equal to the number of tokens in the encoder input times the embedding dimension. This makes sampling from the model challenging, since the molecule length has to be sampled as well. In contrast, learning a fixed-size representation, where all molecules are mapped into the same space, makes sampling easier.

Algorithm 1: Learning parameters $\boldsymbol{\theta}$ of MolMIM

Require: Samples from dataset $\mathcal{P}(\boldsymbol{x})$

while not converged **do**
  $\sigma \sim \mathcal{U}(0, 1]$
  $D_{\text{enc}} \leftarrow \{\boldsymbol{x}_j, \boldsymbol{z}_j \sim q_{\boldsymbol{\theta}}(\boldsymbol{z}|\boldsymbol{x}, \sigma)\mathcal{P}(\boldsymbol{x})\}_{j=1}^{N}$
  $\hat{\mathcal{L}}_{\text{A-MIM}}(\boldsymbol{\theta}; D) = -\frac{1}{N}\sum_{i=1}^{N}\big(\log p_{\boldsymbol{\theta}}(\boldsymbol{x}_i|\boldsymbol{z}_i) + \frac{1}{2}\left(\log q_{\boldsymbol{\theta}}(\boldsymbol{z}_i|\boldsymbol{x}_i, \sigma) + \log \mathcal{P}(\boldsymbol{z}_i)\right)\big)$
  $\Delta\boldsymbol{\theta} \propto -\nabla_{\boldsymbol{\theta}}\hat{\mathcal{L}}_{\text{A-MIM}}(\boldsymbol{\theta}; D)$ {*Gradient computed through sampling using reparameterization*}
end while

Thus, we propose to replace the Transformer encoder with a fixed-sized output Perceiver encoder (Jaegle et al. 2021). Perceiver is an attention-based architecture which utilizes cross-attention to project a variable input onto a fixed-size output. More formally, $\boldsymbol{z} \in \mathbb{R}^H$ for a pre-defined dimension H. We base all proposed models in this paper on the Perceiver architecture.

We train the bottleneck BART using the same learning as a regular BART, which does not explicitly promotes any structure in the learned latent space. We show empirically that BART learns a latent space with "holes", where sampling from a "hole" results in an invalid molecule. As such, in what follows we considered two latent-variable-models (LVMs) which adds a latent regularization to the reconstruction in order to promote structure in the latent space.

Variational Auto Encoder Variational Auto-Encoder (VAE) is a LVM which was introduced by Kingma and Welling (2014). VAE is trained with the following loss per observations,

$$\mathcal{L}_{\text{VAE}}(\boldsymbol{\theta}) = \mathcal{L}_{\text{AE}}(\boldsymbol{\theta}) + \mathcal{D}_{\text{KL}}\left(q_{\boldsymbol{\theta}}(\boldsymbol{z}|\tilde{\boldsymbol{x}}) \,\|\, p_{\boldsymbol{\theta}}(\boldsymbol{z})\right) \tag{2}$$

where $p_{\boldsymbol{\theta}}(\boldsymbol{z})$ is the prior over the the latent code, which is typically a Normal distribution as in our case. The KL divergence term encourages smoothness in the latent space. We define our posterior $q_{\boldsymbol{\theta}}$ to be a Gaussian with a diagonal covariance matrix. We sample $\boldsymbol{z}$ from the posterior using the reparametrization trick which leads to a low variance estimator of the gradient during training.

A main caveat of VAE is a phenomenon called posterior collapse where the learned encoding distribution is closely matching the prior, and the latent codes carry little information (Razavi et al. 2019). Posterior collapse leads to poor reconstruction accuracy, where the learned model performs well as a sampler, but allows little control over the generated molecule. Thus, we consider an alternative LVM in what follows.

Mutual Information Machine Mutual Information Machine (MIM) is a LVM which promotes informative and clustered latent codes (Livne, Swersky, and Fleet 2019). Here we use A-MIM learning (Livne, Swersky, and Fleet

2020), a MIM variant that minimizes the following loss per observation,

$$\mathcal{L}_{\text{MIM}}(\boldsymbol{\theta}) = \mathcal{L}_{\text{AE}}(\boldsymbol{\theta}) + \mathbb{E}_{q_{\boldsymbol{\theta}}}\left[\log\left(p_{\boldsymbol{\theta}}(\boldsymbol{z})q_{\boldsymbol{\theta}}(\boldsymbol{z}|\tilde{\boldsymbol{x}})q_{\boldsymbol{\theta}}(\boldsymbol{x})\right)\right] \quad (3)$$

where the expectation is taken over samples $\boldsymbol{z} \sim q_{\boldsymbol{\theta}}(\boldsymbol{z}|\tilde{\boldsymbol{x}})$, similar to VAE. Minimizing $\mathcal{L}_{\text{A-MIM}}(\boldsymbol{\theta})$ trains a model with a consistent encoder-decoder, high mutual information, and low marginal entropy. We direct the reader to Livne, Swersky, and Fleet (2019) for an in depth explanation of the loss and the various terms.

Unlike VAE, MIM does not suffer from posterior collapse. However, like VAE, it might learn a posterior marginal distribution that does not match the prior, leaving "holes" (Li et al. 2020; Livne, Swersky, and Fleet 2020). Here, we introduce a novel simple extension to A-MIM learning which empirically mitigates the sampling of invalid molecules.

During training, we sample the posterior's standard deviation,

$$q_{\boldsymbol{\theta}}(\boldsymbol{z}|\boldsymbol{x}, \sigma) \equiv \mathcal{N}\big(\boldsymbol{z}|\mu_{\boldsymbol{\theta}}(\boldsymbol{x}), \sigma\big) \quad (4)$$

where $\sigma \sim \mathcal{U}(0, 1]$ is sampled uniformly, and where the posterior is conditioned on the sampled σ via linear mapping which is prepended to the input embedding. This, in effect, is training a model that can accommodate different levels of uncertainty, and is encouraged to learn a dense latent space which supports sampling with little to no "holes". We provide the training procedure in Algorithm 1, where $\mathcal{P}(\boldsymbol{z})$ is a Normal distribution.

In order to understand why such a training procedure would work, it is first important to remember that MIM learning promotes high mutual information (MI) between the observation $\boldsymbol{x}$ and the latent code $\boldsymbol{z}$. The maximization of MI prevents the decoder from ignoring the input latent code. Conditioning the encoder on the variance allows the latent code to carry the uncertainty to the decoder, which then learns to support accurate reconstruction when small variance is provided. For comparison, we applied the same procedure to VAE learning, which led to a complete posterior collapse, where the decoder ignores the latent codes, leading to poor reconstruction.

3 Experiments

In what follows we evaluate the use of a fixed-sized encoder, and latent regularization on small molecule generation. In particular, we trained *MegaMolBART* (NVIDIA 2021), a BART model trained on SMILES data; *PerBART*, a Perceiver BART, where we replace the Transformer encoder with a fixed-size output Perceiver encoder; *MolVAE*, a VAE which shares the architecture with PerBART and has two additional linear layers to project the Perceiver encoder output to a mean and variance of the posterior; and *MolMIM*, a Mutual Information Machine (MIM), a probabilistic autoencoder which shares the same architecture as MolVAE with an additional linear layer to project the provided standard deviation into an input embedding.

Our goal is to assess which architecture and latent space is best suited for novel molecule generation under desired constraints. We evaluate the models in two categories: 1) Sampling quality is measured in terms of validity, uniqueness, and novelty (Sec.3.2). We also introduce a new metric called *effective novelty*, the intersection between the aforementioned metrics, that can be interpreted as "the fraction of useful molecules". 2) Molecule optimization performance is evaluated with constrained single property and multi-objective tasks (Sec. 3.4). We note that we do not explore the effect of model size, hyper-parameters, and data on the models. Instead, we train all models on the same data using the same hyper-parameters, focusing on the effect of the learning framework and the fixed-size bottleneck.

3.1 Training Details

Dataset: All models were trained using a tranche of the ZINC-15 dataset (Sterling and Irwin 2015), labeled as reactive and annotated, with molecular weight $\leq$ 500Da and logP ≤ 5. Of these molecules, 730M were selected at random and split into training, testing, and validation sets, with 723M molecules in the training set.

Data augmentation: Following Irwin et al. (2022), we used two augmentation methods: masking, and SMILES enumeration (Weininger 1988). Masking is as described for the BART MLM denoising objective, with 10% of the tokens being masked and was only used during the training of MegaMolBART. In addition, MegaMolBART, PerBART, and MolVAE used SMILES enumeration where the encoder and decoder received different valid permutations of the input SMILES string. MolMIM was the only model to see an increase in performance when both the encoder and decoder received the same input SMILES permutation, simplifying the training procedure.

Model details: We implemented all models with NeMo Megatron toolkit (Kuchaiev et al. 2019) . We used a RegEx tokenizer with 523 tokens (Bird, Klein, and Loper 2009). All models had 6 layers in the encoder and 6 layers in the decoder, with a hidden size of 512, 8 attention heads, and feed forward dimension of 2048. The Perceiver-based models also required defining K, the hidden length, which relates to the hidden dimension by $H = K \times D$ where H is the total hidden dimension, and D is the model dimension (Fig. 1). MegaMolBART had $58.9M$ parameters, PerBART had $64.6M$, and MolVAE and MolMIM had $65.2M$. We used greedy decoding in all experiments.

Optimization: We use ADAM optimizer (Kingma and Ba 2015) with a learning rate of 1.0, betas of 0.9 and 0.999, weight decay of 0.0, and an epsilon value of 1.0e-8. We used Noam learning rate scheduler (Vaswani et al. 2017) with warm-up ratio 0.008, and a minimum learning rate of 1e-5. During training we used a maximum sequence length of 512, dropout of 0.1, local batch size of 256, and global batch size 16384. All models were trained for 1,000,000 steps with fp16 precision for 40 hours on 4 nodes with 16 GPU/node (Tesla V100 32GB). MolVAE was trained using β-VAE (Higgins et al. 2017) with $\beta = \frac{1}{H}$ where H is the number of hidden dimensions. We have found this choice to provide a reasonable balance between the rate and distortion (see Alemi et al. (2018) for details).

Competing Models For reader convenience we provide here all models that appear in the following tables: CDDD (Winter et al. 2019), JT-VAE (Jin, Barzilay, and Jaakkola 2018), GCPN(You et al. 2018), REINVENT (Olivecrona et al. 2017), GVAE-RL and RationaleRL (Jin, Barzilay, and Jaakkola 2020), MARS (Xie et al. 2021), MolDQN (Zhou et al. 2019), VSeq2Seq (Bahdanau, Cho, and Bengio 2015), VJTNN/VJTNN+GAN (Jin et al. 2019), GA (Nigam et al. 2020), MMPA (Dalke, Hert, and Kramer 2018), AtomG2G and HierG2G (Jin, Barzilay, and Jaakkola 2019), DESMILES (Maragakis et al. 2020), QMO (Hoffman et al. 2022), and GraphDF (Luo, Yan, and Ji 2021).

3.2 Sampling Quality

Our motivation is to be able to sample from our pre-trained models to generate useful molecules for a variety of optimization tasks. To do so, we perturb the latent code of a given molecule by adding Gaussian noise. In more detail, sampling entails

$$\boldsymbol{x}' \sim p_{\boldsymbol{\theta}}(\boldsymbol{x}|\boldsymbol{z}' = \boldsymbol{z} + \epsilon) \tag{5}$$

where the latent code $\boldsymbol{z} = \mathbb{E}_z\left[q_{\boldsymbol{\theta}}(\boldsymbol{z}|\boldsymbol{x})\right]$ is taken to be the posterior mean, and $\epsilon \sim \mathcal{N}\big(\mu = 0, \sigma\big)$ is noise sampled from a Gaussian with a given standard deviation σ. In the case of MegaMolBART and PerBART which have deterministic encoders, we define a posterior as a Dirac delta around the encoder output. We note that such a sampling procedure could benefit from a dense latent space, where random latent codes would map to valid molecules.

In what follows we probe the various models, measuring their sampling performance according to the following common metrics (Brown et al. 2019): *Validity* is the percentage of generated molecules that are valid SMILES[1]; *Uniqueness* is the percentage of generated valid molecules that are unique; and *Novelty* is the percentage of generated valid and unique molecules that are not present in the training data.

Novelty is based on molecules that are not present in the training set. However, it does not discriminate against duplicates. In such a case, one might need to sample multiple times to achieve the desired quantity of novel molecules. For this reason, it can be convenient to have a single metric which describes the sampling efficiency of the model.

As an example, imagine a model reconstructs the novel input molecule 50% of the time, and the other 50% of the time generates different molecules which are valid, novel, and unique. If such a model produces 10 samples, the novelty will be 100%, and uniqueness will be 60%. If the objective is to generate 10 novel molecules, we will have to sample 20 times from this model, which is deceiving for a novelty of 100%.

To address the above issue, and in order to simplify the evaluation of the sampling quality of a model, we introduce two new metrics: *Non-Identicality* is the percentage of valid molecules that are not identical to the input; *Effective Novelty* is the percentage of generated molecules that are valid, non identical, unique, and novel. Effective novelty was created to provide a single metric that measures the percentage of "useful" molecules when sampling, combining all other metrics in a practical manner. In the case of the example above, effective novelty will be 50%. We point the reader to supplementary material for an additional discussion.

Table 1 shows the results of the various sampling metrics, as define above, for best performing models. We performed a grid-search over the hidden length $K \in \{1, 2, 4, 8, 16\}$, and the sampling noise scale $\sigma \in (0, 2]$ (in 0.1 increments) in order to maximize the effective novelty. The results were computed with 10 sampled molecules per input molecule. We randomly sampled 20,000 input molecules from the ZINC-15 test set at the optimal noise scale per model, and report the average sampling metrics.

We conclude, based on Table 1, that the overall sampling quality is improved by the bottleneck architecture of PerBART, and further improved by regularization over the latent codes (*i.e.*, MolMIM, MolVAE). Importantly, MolMIM's best effective novelty was achieved using the smallest number of latent dimensions, which is beneficial for sample-based optimization in the latent space. The usefulness of effective novelty is demonstrated by the CDDD model, which has the best novelty out of all of the benchmarked models, but its effective novelty is 12% lower than MolMIM.

3.3 Latent Space Structure

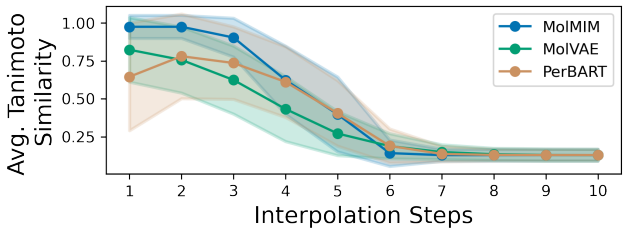

Figure 2: Average Tanimoto similarity (y-axis) between input and non identical interpolated molecules (x-axis is interpolation step). The colored areas mark the corresponding standard deviation. MolMIM clusters similar molecules and shows the smallest variance in the early interpolation steps.

In addition to the ability to sample valid, unique, and novel molecules, we would like to train a model with a learned latent structure that will lend itself to optimization of molecular properties. In the context of unsupervised learning, the structure can relate to similarity of observations, or intrinsic properties of latent codes (*e.g.*, smoothness). We hypothesize that a latent space where latent codes of similar molecules are clustered together will allow for fine-grained control while searching for molecules with target properties.

In what follows we explore the clustering of molecules in the latent space using pair-wise interpolations of 1,000 test set molecules. This allows us to better understand the qualitative differences in the spatial structures of the respective latent spaces of each model. An interpolation entails projecting two molecules onto the latent space by taking the latent codes to be the respective mean of the posterior for each

[1]Validity test is implemented by RDKit: http://www.rdkit.org

Model	K	Latent Dim.	Eff. Nov.(%)	Validity(%)	Unique(%)	Non Id.(%)	Novelty(%)	σ	Test Time	Batch
MMB	-	variable	51.1	75	84.8	74.4	93.1	1.2	8.7 hours	100 †
PerBART	4	2048	59.1	71.8	94.9	88.4	94.3	0.7	38 min	500
MolVAE	4	2048	93.9	95.7	**100**	**100**	98.1	1.2	63 min	500
MolMIM	1	**512**	**94.2**	**98.7**	**100**	99.9	95.5	1.42	**30 min**	500
CDDD	1	**512**	82.2	84.5	98.9	98	**99.4**	1.2	12 hours	1

Table 1: Molecule sampling quality was evaluated with 20,000 molecules randomly selected from the test set, where 10 samples were acquired per molecule. MMB stands for MegaMolBART. K is hidden length. σ is the optimal scale of Gaussian random noise used in sampling. †batch size constrained by memory. Top models are developed herein.

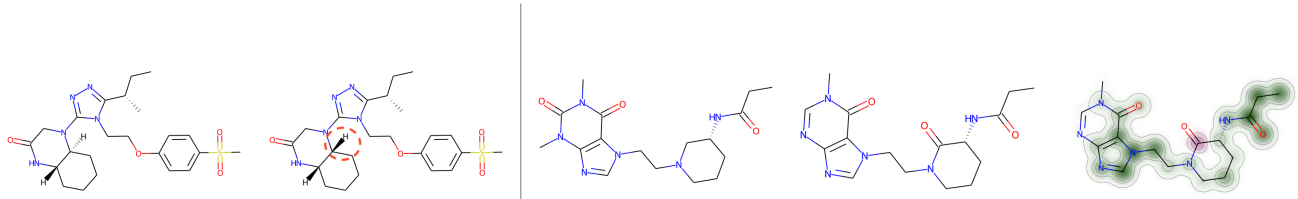

(a) Initial (b) Perturbed (c) Initial (d) Perturbed (e) Similarity Map

Figure 3: MolMIM's fine-grained control over molecule generation. (a-b) Small perturbations lead to changes in chirality only (circled in dashed red). (c-d) Bigger changes allow the substitution of a single atom (red background in similarity map (e)). The similarity map depicts green background for chemically similar structures, and red background for modified structures.

molecule. Following the method used by Gómez-Bombarelli et al. (2018), we then linearly interpolate between the latent codes over 10 equidistant steps, and for each interpolated latent code we decode a corresponding molecule. We then compute the Morgan fingerprint (Rogers and Hahn 2010) with 2048 bits and radius 2, resulting in a bit vector of hashed molecular features for each molecule. Finally, the average Tanimoto similarity (Rogers and Hahn 2010) is calculated between the Morgan fingerprints of the starting and all non-identical interpolated molecules.

Fig. 2 shows that MolVAE's smooth latent space results in a gradual similarity decline, whereas MolMIM contains regions of high similarity followed by a sharp drop off. Notice how MolVAE and PerBART show lower average similarity for interpolation step 1. For MolVAE, it is due to poor reconstruction – adding no noise can result in a different molecule upon decoding. For PerBART, the less ordered structure of its latent space leads to a quick divergence when small amounts of noise is added.

In contrast, MolMIM maintains near perfect similarity for steps 1 and 2, while producing non identical molecules. This is an interesting result as MolMIM is not explicitly trained with similarity information and Tanimoto similarity cannot be calculated directly from SMILES strings (*i.e.*, it requires converting SMILES to Morgan Fingerprints first). We conclude from Fig. 2 that the latent structure of MolMIM is clustered by meaningful chemical similarity.

Fig. 3 depicts qualitative examples of the fine-grained control supported by MolMIM. Fig. 3(a-b) demonstrate how small perturbations can lead to minimal changes, such as inversions of chiral centers of the molecule – *i.e.*, circled in dashed red is a change in chirality only of the molecule. 3(c-e) depict more significant changes where the similarity map highlights in red a single-atom change. The ability to generate molecules of even more diversity is discussed next.

3.4 Small Molecule Optimization

In what follows we use CMA-ES (Hansen 2006), a greedy, gradient-free (*i.e.*, 0^{th} order optimization), evolutionary search algorithm that maximizes a black-box reward function for small molecule optimization. CMA-ES is often used as an optimization baseline (*e.g.*, Yang et al. (2021)), and does not scale well to high-dimensional problems. We apply CMA-ES directly to the latent space to generate proposed latent solutions. These putative solutions are then greedily decoded to generate molecules. The molecules are the required inputs to the reward function, which is comprised of molecular property oracle functions. We used TDC (Huang et al. 2021) oracle functions in order to compute all chemical property values in this section. Here we demonstrate how such a naive algorithm can deliver state-of-the-art results given an informative and clustered latent space.

Single Property Optimization In what follows we explore the optimization of a single chemical property under a Tanimoto similarity constraint δ, which limits the allowed distance from the input molecule. Specifically, we target Quantitative Estimate of Drug-likeness (QED, Bickerton et al. (2012)) and penalized logP (Jin, Barzilay, and Jaakkola 2018).

We use 800 molecules with QED $\in [0.7, 0.8]$ (Jin et al. 2019), and 800 molecules with low penalized logP scores (Jin, Barzilay, and Jaakkola 2018) as the starting points for our respective optimizations. For the QED task, the success

Task	QED (%) $\delta = 0.4$	Penalized logP $\delta = 0.6$	Penalized logP $\delta = 0.4$
JT-VAE	8.8	0.28 ± 0.79	1.03 ± 1.39
GCPN	9.4	0.79 ± 0.63	2.49 ± 1.30
MolDQN	-	1.86 ± 1.21	3.37 ± 1.62
MMPA	32.9	-	-
VSeq2Seq	58.5	2.33 ± 1.17	3.37 ± 1.75
VJTNN+GAN	60.6	-	-
VJTNN	-	2.33 ± 1.24	3.55 ± 1.67
GA	-	3.44 ± 1.09	5.93 ± 1.41
AtomG2G	73.6	-	-
HierG2G	76.9	-	-
DESMILES	77.8	-	-
QMO	92.8	3.73 ± 2.85	7.71 ± 5.65
GraphDF	-	4.51 ± 5.80	9.19 ± 6.43
MolMIM	**94.6**	**7.60 ± 23.62**	**28.45 ± 54.67**
MolMIM†		**4.57 ± 3.87**	**9.44 ± 4.12**

Table 2: QED and penalized logP optimization under similarity constraint δ. QED results show success percentage, and penalized logP show the mean and standard deviation of the improvement in value. † limits logP solutions to improvement ≤ 20. Bottom models are developed herein.

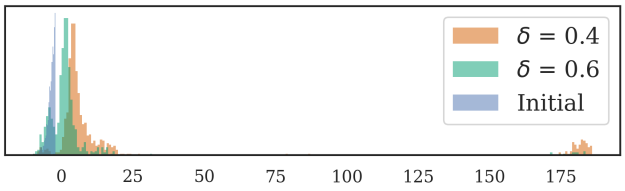

Figure 4: Penalized logP distribution of initial molecules (blue) and optimized molecules under increasingly stringent Tanimoto similarity constraints of 0.6 and 0.4 (green and orange, respectively). The right hand side mode represents a common bias in the penalized logP oracle function.

rate is defined as the percentage of generated molecules with QED ≥ 0.9 while maintaining at least a $\delta = 0.4$ Tanimoto similarity to the respective input (Jin et al. 2019). For the penalized logP task, we report the mean and standard deviation of penalized logP improvement under a similarity constraint for $\delta \in \{0.4, 0.6\}$ (Jin, Barzilay, and Jaakkola 2018). We provide the reward functions and additional information in the supplementary material.

In both experiments we follow a query budget of 50,000 oracle calls per input molecule, following Hoffman et al. (2022). We have found that dividing each optimization into 50 restarts with 1,000 CMA-ES iterations[2], and a population size of 20 to yield the best results. We omit MegaMolBART from the next experiments, since it is unclear how to utilize CMA-ES in a variable size representation. We exclude the results of MolVAE and PerBART from most experiments due to their poor performance and excessively long run time. We point the reader to Table. 3, which is discussed later, as an empirical evidence.

[2]We tested 100, 300, 400, 800, 1000, and 1600 iterations

Model	Success % of QED (iter) 100	300	400	800	Pen. logP ($\delta = 0.4$) avg. Δ	Succ. %
PerBART	2	2.12	-	-	2.6 ± 2.3	23
MolVAE	6.6	21.2	-	-	3.0 ± 2.8	40.6
MolMIM	**37**	**58**	**66.8**	**70.5**	**4.2 ± 1.6**	**78**
CDDD	16	38	51.0	70.2	2.1 ± 2.4	45

Table 3: Results based on compute limited to a single restart and specified number of iterations. Penalized logP uses 100 iterations. Missing results are due to excessively long run time. Top models are developed herein.

Table 2 shows that MolMIM yields new state-of-the-art results in both experiments. We also point the reader to the large value of the standard deviation for the penalized logP experiment. We note that the results are in fact correct, and that MolMIM exploits a known flaw in the logP oracle function where generating molecules with long saturated carbon chains yield high logP values (Renz et al. 2019).

Fig. 4 clearly shows a bimodal distribution with the right hand side mode depicting the logP exploitation described above. As these saturated molecules are not useful in practice (Renz et al. 2019), we also provide results of MolMIM† in Table 2. Here we limit the maximal penalized logP improvement to 20, removing the problematic mode. By doing so we obtain a significantly smaller standard deviation, even compared to competing methods, while still maintaining the highest mean value.

As a final single property experiment, we explore the above tasks using significantly reduced query budgets, and only a single restart. We consider 100, 300, 400, and 800 iterations for the QED task, and 100 iterations for the penalized logP task. Table. 3 shows the results, where MolMIM consistently provides superior results over all other models, including CDDD, which is trained with chemical property information. It is important to mention that only CDDD exhibited generation of invalid molecules during the optimization procedure. We note that the improved performance of both MolMIM and MolVAE, relative to PerBART demonstrates the importance of having a regularized latent space. We also point the reader to the significant difference between MolMIM and MolVAE, demonstrating the importance of the learned latent spaces.

Multi-Objective Property Optimization As a final experiment, we chose a more challenging setting that better represents the complexity of real-world drug discovery (Coley, Eyke, and Jensen 2020). The task is defined over multiple objectives, where a randomly chosen molecule is jointly optimize for QED ≥ 0.6, SA ≤ 4.0, JNK3 ≥ 0.5, and GSK3$\beta \geq 0.5$. We follow the same procedure and model usage as defined by Jin, Barzilay, and Jaakkola (2020) for predicting inhibition of JNK3 and GSK3β.

We consider three variants of initial molecule selection: (R) random start - 2,000 initial molecules are randomly sampled from the ZINC-15 test set; (A) approximate start - 551 initial molecules that satisfy all three conditions QED $\in$

Model	GSK3β + JNK3 + QED + SA		
	Success (%)	Novelty (%)	Diversity
JT-VAE	1.3	-	-
GVAE-RL	2.1	-	-
GCPN	4.0	-	-
REINVENT	47.9	-	-
RationaleRL	74.8	56.1	0.621
MARS	92.3	**82.4**	0.719
MolMIM (R)	**97.5**	71.1	**0.791**
MolMIM (A)	**96.6**	63.3	**0.807**
MolMIM (E)	**98.3**	55.1	**0.767**
MolMIM (E)†	**99.2**	54.8	**0.772**

Table 4: Multi-objective molecule optimization. (R) random initialization, (A) promising precursor initialization, (E) initialization with exemplars. † results are based on additional restarts. Bottom models are developed herein.

$[0.25, 0.4)$, JNK3 $\in [0.25, 0.35)$, GSK3β $\in [0.25, 0.35)$; (E) exemplar-based - 741 initial molecules that already satisfy the required success conditions. In the case of (E), we also force the optimized molecule to have at most 0.4 Tanimoto similarity to the initial molecule. The multi-property experiments entailed 28 restarts of 1500 iterations with a population size of 20. We provide the reward functions in the supplementary material.

Table 4 shows the results measured by success rate, novelty, and diversity, as defined by Jin, Barzilay, and Jaakkola (2020). Here, novelty is the percentage of generated molecules with Tanimoto similarity less than 0.4 compared to the nearest neighbor in the ChEMBL training set (Olivecrona et al. 2017). Diversity is defined as the pairwise Tanimoto similarity over Morgan fingerprints between all generated molecules $1 - \frac{2}{n(n-1)} \sum_{\boldsymbol{x} \neq \boldsymbol{x}'} TanSim(\boldsymbol{x}, \boldsymbol{x}')$ where $\boldsymbol{x}$ is sampled without replacement.

MolMIM clearly improves the success rate, and diversity over all existing methods. MolMIM does not achieve SOTA novelty but does present a significant improvement over RationaleRL. We note that in this case, novelty does not measure the percent of novel generated molecules as done in 3.2. The novelty performance of MARS relative to MolMIM warrants further exploration. A possible explanation for this could involve the use of graph based models by MARS (Xie et al. 2021), which might facilitate the learning of some shape-based molecular features more efficiently than SMILES-based models such as MolMIM.

We also present in Table 4 results for MolMIM (E)†, where we launched additional restarts, reaching to 49 in total. In such a case we present a very high success rate at the expense of diversity. We added MolMIM (E) to mimic more realistic drug development where we generate a new molecular structure while maintaining the desired properties. MolMIM (A) targets drug development use cases where, starting from a promising precursor, we want to generate a successful related molecule.

In summary, we present three variants for multi-objective optimization. MolMIM demonstrates new state-of-the-art results using a simple CMA-ES algorithm, and compares favorably with methods such as MARS, which utilizes a complex Markov chain Monte Carlo sampling algorithm. We attribute the success of MolMIM to the informative and clustered latent space which proved to be useful for various molecule optimization tasks.

4 Related Work

The challenges associated with the task of molecular optimization have resulted in the development of a number of seq2seq models. Several are described below and two will be used for comparison to the models developed in this work.

ChemVAE (Gómez-Bombarelli et al. 2018) was one of the first VAEs developed for querying chemical space. The model learns physical chemical information by jointly training a molecular property predictor from the continuous latent codes during the training of the model. This model, like many SMILES-based models, utilizes character level text encoding. A later model, called CDDD (Winter et al. 2019) which stands for continuous data driven descriptors, has a similar architecture – an auto encoder with regression loss – but was trained on a larger dataset. The model was trained on 72M molecules from ZINC-15 (Sterling and Irwin 2015) and PubChem (Kim et al. 2018), which are two popular publicly available cheminformatics databases.

Chemformer (Irwin et al. 2022), is a seq2seq transformer model based on the BART (Lewis et al. 2020) architecture. This model was trained on 1.45 Billion molecules from ZINC-15 (Sterling and Irwin 2015) – 20X the size of the dataset used to train CDDD. Chemformer can be considered the precursor of the Perceiver based-models described herein.

We propose to utilize a Perceiver (Jaegle et al. 2021) encoder architecture, replacing the usual encoder in BART (Lewis et al. 2020). The Perceiver encoder outputs a fixed-size representation, where molecules of various lengths are mapped into a shared space, allowing us to learn latent variable models (VAE Kingma and Welling (2014), MIM - Mutual Information Machine (Livne, Swersky, and Fleet 2020)).

The effective use of deep learning models for lead optimization also requires a method for efficiently manipulating the model's latent space to generate molecules similar to an example but with improved properties, such as target binding affinity, solubility, reduced toxicity. Previous approaches have employed one of two methods, those which are employed during model training, such as reinforcement learning (Daniel et al. 2018) and grouping molecular transformations pairs with a loss function to predict changes in physical chemical properties (He et al. 2022), and those which are decoupled from training, such as query-based guided search (Hoffman et al. 2022). Our approach, which utilizes CMA-ES, is part of the later group.

5 Conclusions

In this paper we presented a novel probabilistic auto-encoder for small molecules called MolMIM. Trained with Mutual

Information Machine (MIM) learning, the model learns an informative and clustered latent space and samples novel molecules with high probability. We utilize MolMIM to set multiple state-of-the-art results in single and multiple property optimization tasks through the incorporation of a simple search algorithm, CMA-ES. Importantly, any successful solution to the small molecule optimization problem can be applied to other biological modalities such as proteins, RNA, and DNA.

Future research directions will include improvement of the latent space search, replacing CMAE-ES with a more informed search algorithm. In addition, training MolMIM over a graph representation of molecules instead of SMILES might yield further improvement.

6 Acknowledgments

- Danny Reidenbach - Research was performed during an internship at NVIDIA. Danny extended the implementation of the various models, implemented and conducted all experiments, and was instrumental in all aspects of this research. CMA-ES molecular optimization experiments were based on concurrent work at UC Berkeley with Kevin Yang and Dan Klein.
- Micha Livne - Research lead and internship mentor. Micha proposed and designed the research project, implemented the initial models, and was instrumental in all aspects of this research.
- Rajesh K. Ilango - Team member. Implemented the benchmarking framework, and assisted Danny in extending the benchmarking to support the new metrics.
- Michelle Gill - Project technical lead. Michelle was involved in designing the project, implemented the initial MegaMolBART model, and assisted in writing the paper.
- Johnny Israeli - Project sponsor. Johnny was involved in designing the project, and provided valuable feedback during the research and the writing of the paper.

References

Alemi, A.; Poole, B.; Fischer, I.; Dillon, J.; Saurous, R. A.; and Murphy, K. 2018. Fixing a Broken ELBO. In Dy, J.; and Krause, A., eds., *ICML*, volume 80 of *Proceedings of Machine Learning Research*, 159–168. PMLR.

Bahdanau, D.; Cho, K.; and Bengio, Y. 2015. Neural machine translation by jointly learning to align and translate. In *ICLR*.

Berenberg, D.; Lee, J. H.; Kelow, S.; Park, J. W.; Watkins, A.; Gligorijević, V.; Bonneau, R.; Ra, S.; and Cho, K. 2022. Multi-segment preserving sampling for deep manifold sampler.

Bickerton, G. R.; Paolini, G. V.; Besnard, J.; Muresan, S.; and Hopkins, A. L. 2012. Quantifying the chemical beauty of drugs. *Nature Chemistry*, 4(2): 90–98.

Bird, S.; Klein, E.; and Loper, E. 2009. *Natural language processing with Python: analyzing text with the natural language toolkit*. " O'Reilly Media, Inc.".

Brown, N.; Fiscato, M.; Segler, M. H.; and Vaucher, A. C. 2019. GuacaMol: Benchmarking Models for de Novo Molecular Design. *Journal of Chemical Information and Modeling*, 59(3): 1096–1108.

Chuai, G.; Ma, H.; Yan, J.; Chen, M.; Hong, N.; Xue, D.; Zhou, C.; Zhu, C.; Chen, K.; Duan, B.; Gu, F.; Qu, S.; Huang, D.; Wei, J.; and Liu, Q. 2018. DeepCRISPR: optimized CRISPR guide RNA design by deep learning. *Genome Biology*, 19(1): 80.

Coley, C. W.; Eyke, N. S.; and Jensen, K. F. 2020. Autonomous Discovery in the Chemical Sciences Part II: Outlook. *Angewandte Chemie International Edition*, 59(52): 23414–23436.

Dalke, A.; Hert, J.; and Kramer, C. 2018. mmpdb: An Open-Source Matched Molecular Pair Platform for Large Multiproperty Data Sets. *Journal of Chemical Information and Modeling*, 58(5): 902–910.

Daniel, N.; Marwin, S.; Laura, G.; Mohamed, A.; Dean, P.; Matthew, S.; and Brown, N. 2018. Exploring Deep Recurrent Models with Reinforcement Learning for Molecule Design.

Engkvist, O.; Arús-Pous, J.; Bjerrum, E. J.; and Chen, H. 2021. Chapter 13 Molecular De Novo Design Through Deep Generative Models. In *Artificial Intelligence in Drug Discovery*, 272–300. The Royal Society of Chemistry. ISBN 978-1-78801-547-9.

Ertl, P.; and Schuffenhauer, A. 2009. Estimation of synthetic accessibility score of drug-like molecules based on molecular complexity and fragment contributions. *Journal of Cheminformatics*, 1(1): 8.

Goodfellow, I.; Bengio, Y.; and Courville, A. 2016. *Deep Learning*. MIT Press. http://www.deeplearningbook.org.

Gómez-Bombarelli, R.; Wei, J. N.; Duvenaud, D.; Hernández-Lobato, J. M.; Sánchez-Lengeling, B.; Sheberla, D.; Aguilera-Iparraguirre, J.; Hirzel, T. D.; Adams, R. P.; and Aspuru-Guzik, A. 2018. Automatic Chemical Design Using a Data-Driven Continuous Representation of Molecules. *ACS Central Science*, 4(2): 268–276. PMID: 29532027.

Hansen, N. 2006. The CMA Evolution Strategy: A Comparing Review.

He, J.; Nittinger, E.; Tyrchan, C.; Czechtizky, W.; Patronov, A.; Bjerrum, E. J.; and Engkvist, O. 2022. Transformer-based molecular optimization beyond matched molecular pairs. *Journal of Cheminformatics*, 14(1): 18.

Higgins, I.; Matthey, L.; Pal, A.; Burgess, C.; Glorot, X.; Botvinick, M.; Mohamed, S.; and Lerchner, A. 2017. beta-VAE: Learning Basic Visual Concepts with a Constrained Variational Framework. In *ICLR*.

Hoffman, S. C.; Chenthamarakshan, V.; Wadhawan, K.; Chen, P.-Y.; and Das, P. 2022. Optimizing molecules using efficient queries from property evaluations. *Nature Machine Intelligence*, 4(1): 21–31.

Huang, K.; Fu, T.; Gao, W.; Zhao, Y.; Roohani, Y.; Leskovec, J.; Coley, C. W.; Xiao, C.; Sun, J.; and Zitnik, M. 2021. Therapeutics Data Commons: Machine Learning

Datasets and Tasks for Drug Discovery and Development. *NeurIPS Datasets and Benchmarks*.

Irwin, R.; Dimitriadis, S.; He, J.; and Bjerrum, E. J. 2022. Chemformer: a pre-trained transformer for computational chemistry. *Machine Learning: Science and Technology*, 3(1): 015022.

Jaegle, A.; Gimeno, F.; Brock, A.; Vinyals, O.; Zisserman, A.; and Carreira, J. 2021. Perceiver: General Perception with Iterative Attention. In Meila, M.; and Zhang, T., eds., *Proceedings of the 38th International Conference on Machine Learning*, volume 139 of *Proceedings of Machine Learning Research*, 4651–4664. PMLR.

Jin, W.; Barzilay, D.; and Jaakkola, T. 2020. Multi-Objective Molecule Generation using Interpretable Substructures. In III, H. D.; and Singh, A., eds., *ICML*, volume 119 of *Proceedings of Machine Learning Research*, 4849–4859. PMLR.

Jin, W.; Barzilay, R.; and Jaakkola, T. 2018. Junction Tree Variational Autoencoder for Molecular Graph Generation. In Dy, J.; and Krause, A., eds., *ICML*, volume 80 of *Proceedings of Machine Learning Research*, 2323–2332. PMLR.

Jin, W.; Barzilay, R.; and Jaakkola, T. 2019. Hierarchical Graph-to-Graph Translation for Molecules.

Jin, W.; Yang, K.; Barzilay, R.; and Jaakkola, T. 2019. Learning Multimodal Graph-to-Graph Translation for Molecule Optimization. In *ICLR*.

Kim, H.; Kim, E.; Lee, I.; Bae, B.; Park, M.; and Nam, H. 2020. Artificial intelligence in drug discovery: A comprehensive review of data-driven and machine learning approaches. *Biotechnol. Bioprocess Eng.*, 25(6): 895–930.

Kim, S.; Chen, J.; Cheng, T.; Gindulyte, A.; He, J.; He, S.; Li, Q.; Shoemaker, B. A.; Thiessen, P. A.; Yu, B.; Zaslavsky, L.; Zhang, J.; and Bolton, E. E. 2018. PubChem 2019 update: improved access to chemical data. *Nucleic Acids Research*, 47(D1): D1102–D1109.

Kingma, D. P.; and Ba, J. 2015. Adam: A Method for Stochastic Optimization. In Bengio, Y.; and LeCun, Y., eds., *ICLR*.

Kingma, D. P.; and Welling, M. 2014. Auto-Encoding Variational Bayes. *CoRR*, abs/1312.6114.

Kuchaiev, O.; Li, J.; Nguyen, H.; Hrinchuk, O.; Leary, R.; Ginsburg, B.; Kriman, S.; Beliaev, S.; Lavrukhin, V.; Cook, J.; et al. 2019. Nemo: a toolkit for building ai applications using neural modules. *arXiv preprint arXiv:1909.09577*.

Lewis, M.; Liu, Y.; Goyal, N.; Ghazvininejad, M.; Mohamed, A.; Levy, O.; Stoyanov, V.; and Zettlemoyer, L. 2020. BART: Denoising Sequence-to-Sequence Pre-training for Natural Language Generation, Translation, and Comprehension. In *ACL*, 7871–7880. Online: Association for Computational Linguistics.

Li, R.; Peng, X.; Lin, C.; Rong, W.; and Chen, Z. 2020. On the Low-density Latent Regions of VAE-based Language Models. In Bertinetto, L.; Henriques, J. F.; Albanie, S.; Paganini, M.; and Varol, G., eds., *NeurIPS Workshop on Preregistration in Machine Learning*, volume 148 of *Proceedings of Machine Learning Research*, 343–357. PMLR.

Livne, M.; Swersky, K.; and Fleet, D. J. 2019. MIM: Mutual Information Machine. *arXiv e-prints*.

Livne, M.; Swersky, K.; and Fleet, D. J. 2020. SentenceMIM: A Latent Variable Language Model.

Luo, Y.; Yan, K.; and Ji, S. 2021. GraphDF: A Discrete Flow Model for Molecular Graph Generation. In Meila, M.; and Zhang, T., eds., *ICML*, volume 139 of *Proceedings of Machine Learning Research*, 7192–7203. PMLR.

Mahmood, O.; Mansimov, E.; Bonneau, R.; and Cho, K. 2021. Masked graph modeling for molecule generation. *Nature Communications*, 12(1): 3156.

Maragakis, P.; Nisonoff, H.; Cole, B.; and Shaw, D. E. 2020. A Deep-Learning View of Chemical Space Designed to Facilitate Drug Discovery. *Journal of Chemical Information and Modeling*, 60(10): 4487–4496.

Nigam, A.; Friederich, P.; Krenn, M.; and Aspuru-Guzik, A. 2020. Augmenting Genetic Algorithms with Deep Neural Networks for Exploring the Chemical Space. In *ICLR*.

NVIDIA. 2021.

Olivecrona, M.; Blaschke, T.; Engkvist, O.; and Chen, H. 2017. Molecular de-novo design through deep reinforcement learning. *Journal of Cheminformatics*, 9(1): 48.

Razavi, A.; van den Oord, A.; Poole, B.; and Vinyals, O. 2019. Preventing Posterior Collapse with delta-VAEs. In *ICLR*.

Renz, P.; Van Rompaey, D.; Wegner, J. K.; Hochreiter, S.; and Klambauer, G. 2019. On failure modes in molecule generation and optimization. *Drug Discovery Today: Technologies*, 32-33: 55–63.

Rogers, D.; and Hahn, M. 2010. Extended-Connectivity Fingerprints. *Journal of Chemical Information and Modeling*, 50(5): 742–754. PMID: 20426451.

Sliwoski, G.; Kothiwale, S.; Meiler, J.; and Lowe, E. W. 2014. Computational Methods in Drug Discovery. *Pharmacological Reviews*, 66(1): 334–395.

Sterling, T.; and Irwin, J. J. 2015. ZINC 15 – Ligand Discovery for Everyone. *Journal of Chemical Information and Modeling*, 55(11): 2324–2337.

Vamathevan, J.; Clark, D.; Czodrowski, P.; Dunham, I.; Ferran, E.; Lee, G.; Li, B.; Madabhushi, A.; Shah, P.; Spitzer, M.; and Zhao, S. 2019. Applications of machine learning in drug discovery and development. *Nature Reviews Drug Discovery*, 18(6): 463–477.

Vaswani, A.; Shazeer, N.; Parmar, N.; Uszkoreit, J.; Jones, L.; Gomez, A. N.; Kaiser, L. u.; and Polosukhin, I. 2017. Attention is All you Need. In Guyon, I.; Luxburg, U. V.; Bengio, S.; Wallach, H.; Fergus, R.; Vishwanathan, S.; and Garnett, R., eds., *Advances in Neural Information Processing Systems*, volume 30. Curran Associates, Inc.

Weininger, D. 1988. SMILES, a chemical language and information system. 1. Introduction to methodology and encoding rules. *Journal of Chemical Information and Computer Sciences*, 28(1): 31–36.

Winter, R.; Montanari, F.; Noé, F.; and Clevert, D.-A. 2019. Learning continuous and data-driven molecular descriptors

by translating equivalent chemical representations. *Chemical Science*, 10: 1692–1701.

Xie, Y.; Shi, C.; Zhou, H.; Yang, Y.; Zhang, W.; Yu, Y.; and Li, L. 2021. MARS: Markov Molecular Sampling for Multi-objective Drug Discovery. In *ICLR*.

Yang, K.; Zhang, T.; Cummins, C.; Cui, B.; Steiner, B.; Wang, L.; Gonzalez, J. E.; Klein, D.; and Tian, Y. 2021. Learning Space Partitions for Path Planning. In Beygelzimer, A.; Dauphin, Y.; Liang, P.; and Vaughan, J. W., eds., *NeurIPS*.

You, J.; Liu, B.; Ying, R.; Pande, V.; and Leskovec, J. 2018. Graph Convolutional Policy Network for Goal-Directed Molecular Graph Generation. In *NeurIPS*, NIPS'18, 6412–6422. Red Hook, NY, USA: Curran Associates Inc.

Zhou, Z.; Kearnes, S.; Li, L.; Zare, R. N.; and Riley, P. 2019. Optimization of Molecules via Deep Reinforcement Learning. *Sci Rep*, 9(1): 10752.

A Supplementary Material

A.1 Small Molecule Optimization

In this section we formulate the reward functions that were used in the small molecule optimization part of the main body.

Single Property Optimization Quantitative Estimate of Druglikeness (QED) is a simple rule-based molecular property that measures drug-likeliness (Bickerton et al. 2012). Penalized logP (Jin, Barzilay, and Jaakkola 2018) is logP[3] minus the Synthetic Accessibility (SA) score (Ertl and Schuffenhauer 2009).

Formally, we define the following reward functions for our CMA-ES optimization:

$$\mathcal{R}_{QED} = \min(\frac{QED}{0.9}, 1) + \min(\frac{TanSim}{0.4}, 1) \quad (6)$$

$$\mathcal{R}_{plogP} = \frac{plogP}{20} + \min(\frac{TanSim}{\delta}, 1) \quad (7)$$

where $TanSim$ is the Tanimoto similarity, δ is the value of the similarity constraint, and QED, $plogP$ are the corresponding properties. Loss scaling of each term was tuned manually over a few test runs.

Multi Property Property Optimization JNK3 is the inhibition of c-Jun N-terminal kinase-3. GSK3β is the inhibition of glycogen synthase kinase-3 beta.

Formally, we show the reward function below,

$$\mathcal{R}^{R,A}_{MP} = \frac{QED + GSK3\beta}{2} + \frac{SA}{40} + JNK3 \quad (8)$$

$$\mathcal{R}^{E}_{MP} = \frac{1}{50}\mathcal{R}^{R,A}_{MP} + \min(1.0, \frac{1 - TanSim}{1 - 0.4}) \quad (9)$$

where $TanSim$ is the Tanimoto similarity, and QED, SA, $JNK3$, $GSK3\beta$ are the corresponding properties. Loss scaling of each term was tuned manually over a few test runs.

A.2 Finding Optimal Noise Scale for Top Models

In this section we show the results of hyper-parameter search for the optimal noise scale that maximizes effective novelty, per model. See Figs. 5, 6, 7, 8, 9. We omit here the search for the optimal hidden length K per model, where we considered $K \in 1, 2, 4, 8, 16$ for all models.

[3]logP is the $\log_{10}$ of the octanol and water solute partition ratio and is a measure of hydrophobicity with larger values indicating increased hydrophobicity.

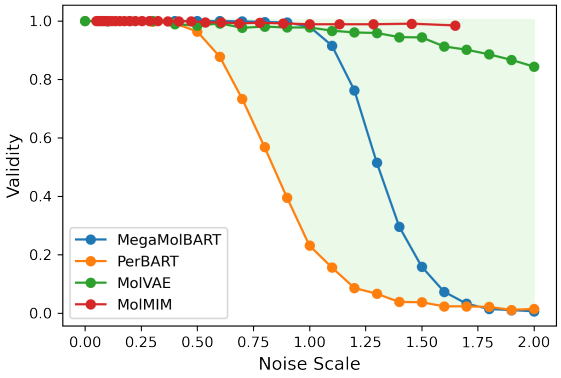

Figure 5: Validity as a function of noise scale. Note how latent variable models, MolVAE and MolMIM, are consistent while the others, MegaMolBART and PerBART, see a sharp decline at larger noise scales.

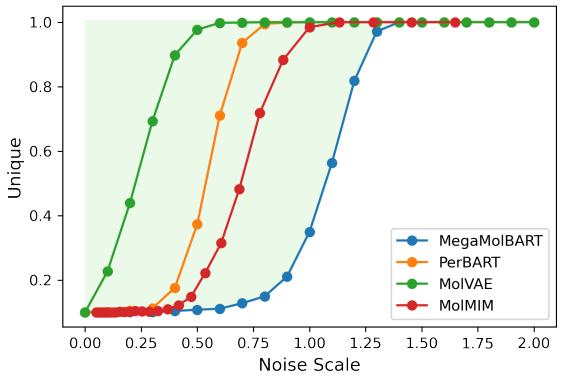

Figure 6: Uniqueness as a function of noise scale. Note MegaMolBART is a lower bound for the entire range of tested noise scales.

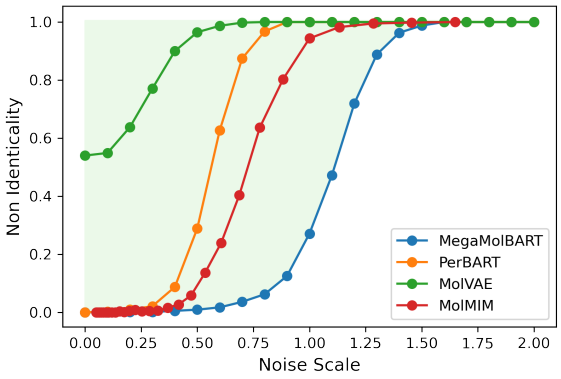

Figure 7: Non Identicality as a function of noise scale. Note at a nose scale of 0, only MolVAE has a non zero non identicality as a result of poor reconstruction (*i.e.*, relates to posterior collapse).

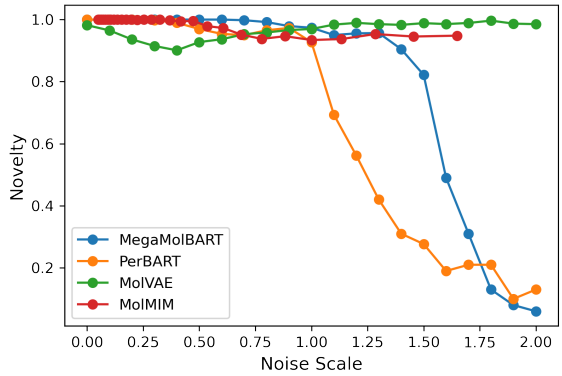

Figure 8: Novelty as a function of noise scale. Note how latent variable models, MolVAE and MolMIM, are consistent while the others, MegaMolBART and PerBART, see a sharp decline due to the increased validity issues at large noise scales.

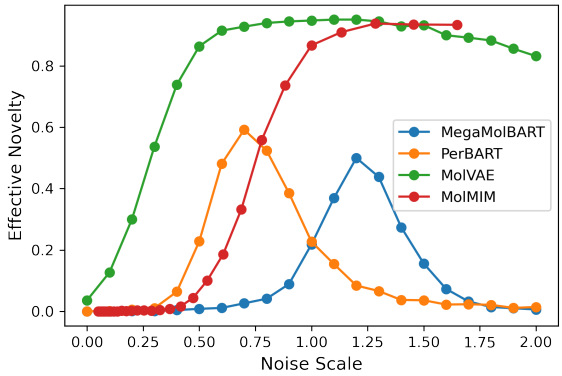

Figure 9: Effective Novelty as a function of noise scale. Note the non latent variable models, MegaMolBART and PerBART, have a parabolic shape due to validity issues at large noise scales.

A.3 Sampling Metrics

Sampling Metric Formulation Here, we formulate the sampling metrics as described in the main body:

$$\text{validity} = \frac{|V|}{|G|} \tag{10}$$

$$\text{uniqueness} = \frac{|U|}{|V|} \tag{11}$$

$$\text{novelty} = \frac{|N|}{|U|} \tag{12}$$

$$\text{non identicality} = \frac{|\bar{I}|}{|V|} \tag{13}$$

$$\text{effective novelty} = \frac{|N \cap \bar{I}|}{|G|} \tag{14}$$

where

- G is the set of all generated molecules
- V is the subset of all valid molecules in G
- U is the subset of all unique molecules in V
- N is the subset of all novel molecules in U
- $\bar{I}$ is the subset of all non identical molecules in V

are the corresponding sets.

The design flaw in Eq. 12 is that N is a subset of U and therefore does not consider the total amount of generated molecules G. Effective novelty not only measures the percentage of useful molecules but it also provides a measurement for sampling efficiency as it is defined over all generated molecules in Eq. 14.

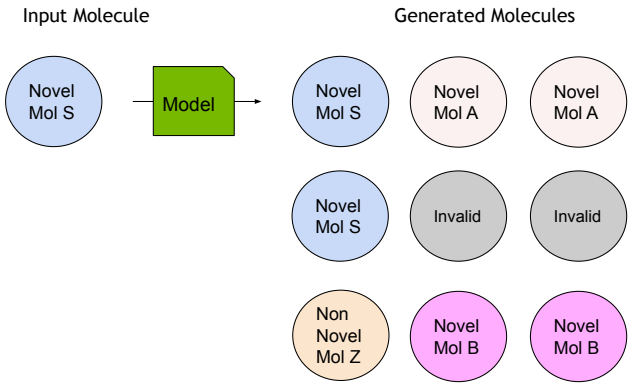

Figure 10: Given a novel input molecule S, we provide an example sampling output used in Figure. 11 to visualize all of the defined metrics Eq. 10 - 14

Visualizing Effective Novelty We provide depiction of effective novelty in Figs. 10-11.

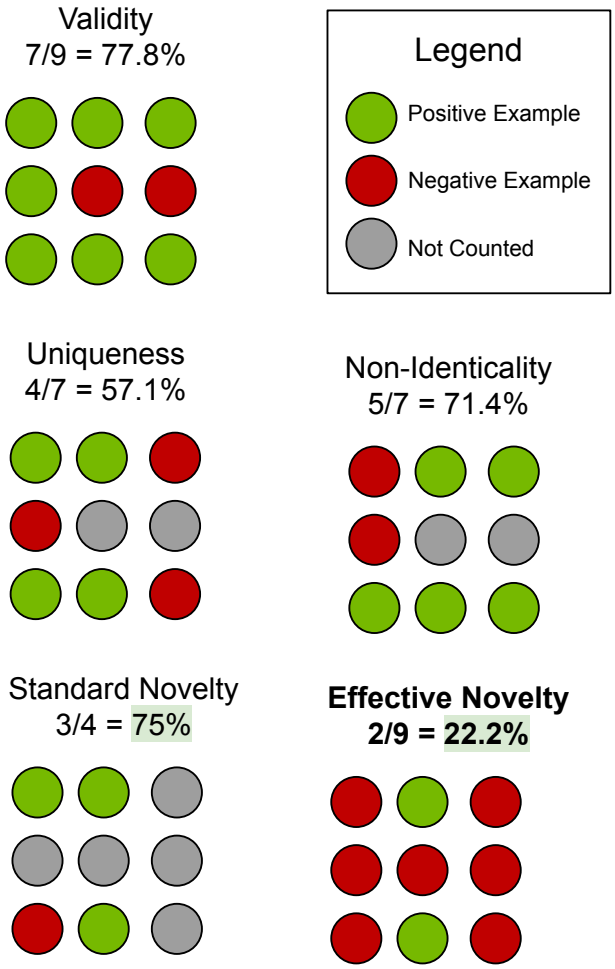

Figure 11: Here we highlight the difference between novelty and effective novelty. For each metric we mark the numerator (green), denominator (green + red), and the irrelevant part(gray). High novelty might still lead to low efficiency in sampling novel molecules.